Power and limitations of single-qubit native quantum neural networks

Anonymous Author(s)
Affiliation
Address
email

Abstract

Quantum neural networks (QNNs) have emerged as a leading strategy to establish applications in machine learning, chemistry, and optimization. While the applications of QNN have been widely investigated, its theoretical foundation remains less understood. In this paper, we formulate a theoretical framework for the expressive ability of data re-uploading quantum neural networks that consist of interleaved encoding circuit blocks and trainable circuit blocks. First, we prove that single-qubit quantum neural networks can approximate any univariate function by mapping the model to a partial Fourier series. We in particular establish the exact correlations between the parameters of the trainable gates and the Fourier coefficients, resolving an open problem on the universal approximation property of QNN. Second, we discuss the limitations of single-qubit native QNNs on approximating multivariate functions by analyzing the frequency spectrum and the flexibility of Fourier coefficients. We further demonstrate the expressivity and limitations of single-qubit native QNNs via numerical experiments. We believe these results would improve our understanding of QNNs and provide a helpful guideline for designing powerful QNNs for machine learning tasks.

1 Introduction

Quantum computing is a technology that exploits the laws of quantum mechanics to solve complicated problems much faster than classical computers. It has been applied in areas such as breaking cryptographic systems [1], searching databases Grover [2], and quantum simulation [3, 4], in which it gives a quantum speedup over the best known classical algorithms. With the fast development of quantum hardware, recent results [5–7] have shown quantum advantages in specific tasks. An emerging direction is to investigate if quantum computing can offer quantum advantages in artificial intelligence, giving rise to an interdisciplinary area called *quantum machine learning* [8].

A leading strategy to quantum machine learning uses *quantum neural networks* (QNNs), which are quantum analogs of artificial neural networks (NNs). Much progress has been made in applications of QNN in various topics [9–11], including quantum autoencoder [12, 13], supervised learning [14–17], dynamic learning [18–20], quantum chemistry [21], and quantum metrology [22–24]. Similar to the field of machine learning, a crucial challenge of quantum machine learning is to design powerful and efficient QNN models for quantum learning tasks, which requires a theoretical understanding of how structural properties of QNN may affect its expressive power.

The expressive power of a QNN model can be characterized by the function classes that it can approximate. Recently, the universal approximation property (UAP) of QNN models has been investigated, which is similar to the universal approximation theorem [25, 26] in machine learning theory. The authors of [27] suggested that a QNN model can be written as a partial Fourier series in the data and proved the existence of a multi-qubit QNN model that can realize a universal function

Submitted to 36th Conference on Neural Information Processing Systems (NeurIPS 2022). Do not distribute.

approximator. The UAP of single-qubit models remains an open conjecture, due to the difficulties in analyzing the flexibility of Fourier coefficients. Another work [28] considered hybrid classical-quantum neural networks and obtained the UAP by using the Stone-Weierstrass theorem. Ref. [29] proved that even a single-qubit hybrid QNN can approximate any bounded function.

The above results of UAP show that the expressivity of QNNs is strong, but it does not reveal the relationship between the structural properties of a QNN and its expressive ability. Therefore the UAP may not be a good guide for constructing QNN models with practical interests. In particular, it is worth noting that the existence proof in Ref. [27] is under the assumption of multi-qubit systems, exponential circuit depth, and arbitrary observables, which does not explicitly give the structure of QNNs. Meanwhile, Refs. [28, 29] demonstrated the construction of QNNs in detail, but it is unclear whether the powerful expressivity comes from the classical part or the quantum part of hybrid models. Moreover, a systematic analysis of how parameters in the QNN affect the classes of functions that it can approximate is missing. The absence of these theoretical foundations hinders the understanding on the expressive power and limitation of QNNs, which makes it highly necessary but challenging to design effective and efficient QNNs.

To theoretically investigate the expressivity of QNNs, it is important to study the simplest case of single-qubit QNNs, just like the celebrated universal approximation theorem first showing the expressivity of depth-2 NNs [25, 26]. In this paper, we formulate an analytical framework that correlates the structural properties of a single-qubit native QNN and its expressive power. We consider data re-uploading models that consist of interleaved data encoding circuit blocks and trainable circuit blocks [30]. First, we prove that there exists a single-qubit native QNN that can express any Fourier series, which is a universal approximator for any square-integrable univariate function. It solves the open problem on the UAP of single-qubit QNNs in Ref. [27]. Second, we systematically analyze how parameters in trainable circuit blocks affect the Fourier coefficients. The main results on the expressivity of QNNs are summarized as in Fig. 1. Third, we discuss potential difficulties for single-qubit native QNNs to approximate multivariate functions. Additionally, we compare native QNNs with the hybrid version and show the fundamental difference in their expressive power. We also demonstrate the expressivity and limitations of single-qubit native QNNs via numerical experiments on approximating univariate and multivariate functions. Our analysis, beyond the UAP of QNNs, improves the understanding of the relationship between the expressive power and the structure of QNNs. This fundamental framework provides a theoretical foundation for data re-uploading QNN models, which is helpful to construct effective and efficient QNNs for quantum machine learning tasks.

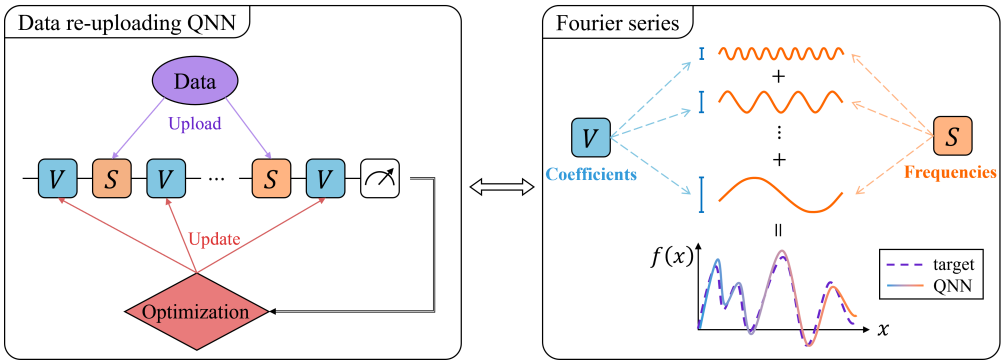

Figure 1: **A schematic diagram of the main results.** A single-qubit data re-uploading QNN model consisting of interleaved trainable blocks (in blue) and encoding blocks (in orange) corresponds to a partial Fourier series. The encoding blocks decide the frequency spectrum of the Fourier series and the trainable blocks control the Fourier coefficients. By the summability and convergence of the Fourier series, the QNN model can approximate any square-integrable target function.

We will start by giving some background and defining the native QNN models in the next section, and then analyze the expressivity of single-qubit native QNNs in Section 3. In Section 4, we discuss the limitation of single-qubit native QNNs and compare native QNNs with hybrid QNNs, which shows the fundamental difference between their expressive power. The numerical experiments on the expressivity and limitations of single-qubit native QNNs are described in Section 5.

2 Preliminaries

2.1 A primer on quantum computing

Quantum state The basic unit of information in quantum computation is one *quantum bit*, or *qubit* for short. Just like a classical bit has a state in either 0 or 1, a qubit also has a state. A single-qubit state is a unit vector in a 2-dimensional Hilbert space $\mathbb{C}^2$, which is commonly denoted in Dirac notation $|\psi\rangle = \alpha|0\rangle + \beta|1\rangle$, where $|0\rangle = (1,0)^T$ and $|1\rangle = (0,1)^T$ are known as computational basis states. Here $|\psi\rangle$ denotes a column vector and its conjugate transpose $\langle\psi| := |\psi\rangle^\dagger$ is a row vector. Then the inner product $\langle\psi|\psi\rangle = \|\psi\|^2$ denotes the square of L^2-norm of $|\psi\rangle$. Note that $|\psi\rangle$ is a normalized state so $\langle\psi|\psi\rangle = |\alpha|^2 + |\beta|^2 = 1$. Having this constraint, a single-qubit state can be represented as a point at surface of a *Bloch sphere*, written as $|\psi\rangle = \cos(\theta/2)|0\rangle + e^{i\phi}\sin(\theta/2)|1\rangle$, where θ and ϕ are re-interpreted as azimuthal angle and polar angle in spherical coordinates. More generally, a quantum state of n qubits can be represented as a normalized vector in the n-fold tensor product Hilbert space $\mathbb{C}^{2^n}$.

Quantum gate Quantum gates are basic operations used to manipulate qubits. Unlike some classical logical gates, quantum gates are reversible, so they can be represented as *unitary transformations* in the Hilbert space. A unitary matrix U satisfies $U^\dagger U = UU^\dagger = I$. A commonly used group of single-qubit quantum gates is the *Pauli gates*, which can be written as Pauli matrices:

$$X = \begin{bmatrix} 0 & 1 \\ 1 & 0 \end{bmatrix}, \qquad Y = \begin{bmatrix} 0 & -i \\ i & 0 \end{bmatrix}, \qquad Z = \begin{bmatrix} 1 & 0 \\ 0 & -1 \end{bmatrix}. \tag{1}$$

The Pauli X, Y, and Z gates are equivalent to a rotation around the x, y, and z axes of the Bloch sphere by π radians, respectively. A group of more general gates is the *rotation operator gates* $\{R_P(\theta) = e^{-i\frac{\theta}{2}P} \mid P \in \{X, Y, Z\}\}$, which allows the rotating angle around the x, y and z axes of the Bloch sphere to be customized. They can be written in the matrix form as

$$R_X(\theta) = \begin{bmatrix} \cos\frac{\theta}{2} & -i\sin\frac{\theta}{2} \\ -i\sin\frac{\theta}{2} & \cos\frac{\theta}{2} \end{bmatrix}, \quad R_Y(\theta) = \begin{bmatrix} \cos\frac{\theta}{2} & -\sin\frac{\theta}{2} \\ \sin\frac{\theta}{2} & \cos\frac{\theta}{2} \end{bmatrix}, \quad R_Z(\theta) = \begin{bmatrix} e^{-i\frac{\theta}{2}} & 0 \\ 0 & e^{i\frac{\theta}{2}} \end{bmatrix}. \tag{2}$$

Quantum measurement A measurement is a quantum operation to retrieve classical information from a quantum state. The simplest measurement is the computational basis measurement; for a single-qubit state $|\psi\rangle = \alpha|0\rangle + \beta|1\rangle$, the outcome of such a measurement is either $|0\rangle$ with probability $|\alpha|^2$ or $|1\rangle$ with probability $|\beta|^2$. Computational basis measurements can be generalized to *Pauli measurements*, where Pauli matrices are *observables* that we can measure. For example, measuring Pauli Z is equivalent to the computational basis measurement, since $|0\rangle$ and $|1\rangle$ are eigenvectors of Z with corresponding eigenvalues ± 1. Pauli Z measurement returns $+1$ if the resulting state is $|0\rangle$ and returns -1 if the resulting state is $|1\rangle$. We can calculate the expected value of Pauli Z measurement when the state is $|\psi\rangle$:

$$\langle\psi| Z |\psi\rangle = (\alpha^* \langle 0| + \beta^* \langle 1|)Z(\alpha|0\rangle + \beta|1\rangle) = |\alpha|^2 - |\beta|^2. \tag{3}$$

Pauli measurements can be extended to the case of multiple qubits by a tensor product of Pauli matrices.

2.2 Data re-uploading quantum neural networks

We consider the data re-uploading QNN model [30], which is a generalized framework of quantum machine learning models based on parameterized quantum circuits [31]. A data re-uploading QNN is a quantum circuit that consists of interleaved data encoding circuit blocks $S(\cdot)$ and trainable circuit blocks $V(\cdot)$,

$$U_{\boldsymbol{\theta},L}(\boldsymbol{x}) = V(\boldsymbol{\theta_0}) \prod_{j=1}^{L} S(\boldsymbol{x}) V(\boldsymbol{\theta_j}), \tag{4}$$

where $\boldsymbol{x}$ is the input data, $\boldsymbol{\theta} = (\boldsymbol{\theta_0}, \ldots, \boldsymbol{\theta_L})$ is a set of trainable parameters, and L denotes the number of layers. It is common to build the data encoding blocks and trainable blocks using the most

prevalent parameterized quantum operators $\{R_X, R_Y, R_Z\}$. We define the output of this model as the expectation value of measuring some observable M,

$$f_{\boldsymbol{\theta},L}(\boldsymbol{x}) = \langle 0| U^\dagger_{\boldsymbol{\theta},L}(\boldsymbol{x}) M U_{\boldsymbol{\theta},L}(\boldsymbol{x}) |0\rangle . \tag{5}$$

Note that some data re-uploading QNNs introduce trainable weights in data pre-processing or post-processing, which are considered as hybrid QNNs. For example, the data encoding block defined as $S(\boldsymbol{w} \cdot \boldsymbol{x})$ is essentially equivalent to feeding data $\boldsymbol{x}$ into a neuron with weight $\boldsymbol{w}$ and then uploading the output to an encoding block $S(\cdot)$. Such a mixing structure makes it hard to tell whether the expressive power comes from the classical or quantum part. To solely study the expressive power of QNNs, we define the concept of *native QNN*, where all trainable weights are introduced by parameters of tunable quantum gates so that they can be distinguished from a hybrid QNN. Throughout this paper, we simply refer to the native QNN as QNN for short unless specified otherwise.

3 Expressivity of single-qubit QNNs

To better understand the expressive power of QNNs, we start investigating the simplest case of single-qubit models. Ref. [27] investigated the expressive power of QNNs using the Fourier series formalism. In this section, we establish an exact correlation between the single-qubit QNN and the Fourier series in terms of both the frequency spectrum and Fourier coefficients. Note that we consider one-dimensional input data for now, which corresponds to the class of univariate functions.

A Fourier series is an expansion of a periodic function $f(x)$ in infinite terms of a sum of sines and cosines which can be written in the exponential form as

$$f(x) = \sum_{n=-\infty}^{\infty} c_n e^{i\frac{2\pi}{T}nx}, \tag{6}$$

where

$$c_n = \frac{1}{T}\int_T f(x) e^{i\frac{2\pi}{T}nx} dx \tag{7}$$

are the Fourier coefficients. Here T is the period of function $f(x)$. The quantities $n\frac{2\pi}{T}$ are called the *frequencies*, which are multiples of the base frequency $\frac{2\pi}{T}$. The set of frequency $\{n\frac{2\pi}{T}\}_n$ is called the *frequency spectrum* of Fourier series.

In approximation theory, a partial Fourier series (or truncated Fourier series)

$$s_N(x) = \sum_{n=-N}^{N} c_n e^{i\frac{\pi}{T}nx} \tag{8}$$

is commonly used to approximate the function $f(x)$. A partial Fourier series can be transformed to a Laurent polynomial $P \in \mathbb{C}[z, z^{-1}]$ by the substitution $z = e^{i\frac{2\pi}{T}x}$, i.e.,

$$P(z) = \sum_{n=-N}^{N} c_n z^n. \tag{9}$$

A Laurent polynomial $P \in \mathbb{F}[z, z^{-1}]$ is a linear combination of positive and negative powers of the variable z with coefficients in $\mathbb{F}$. The *degree* of a Laurent polynomial P is the maximum absolute value of any exponent of z with non-zero coefficients, denoted by $\deg(P)$. We say that a Laurent polynomial P has *parity* 0 if all coefficients corresponding to odd powers of z are 0, and similarly P has parity 1 if all coefficients corresponding to even powers of z are 0.

Following the pattern of Fourier series, we first consider using $R_Z(x) = e^{-ixZ/2}$ to encode the input x and let $R_Y(\cdot)$ be the trainable gate. We can write the QNN as

$$U^{YZY}_{\boldsymbol{\theta},L}(x) = R_Y(\theta_0) \prod_{j=1}^{L} R_Z(x) R_Y(\theta_j), \tag{10}$$

and the quantum circuit is shown in Fig. 2.

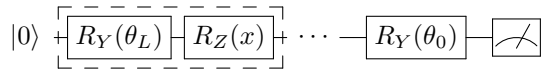

Figure 2: Circuit of $U^{YZY}_{\boldsymbol{\theta},L}(x)$, where the trainable block is $R_Y(\cdot)$ and the encoding block is $R_Z(\cdot)$.

To characterize the expressivity of this kind of basic QNN, we first rigorously show that the QNN $U^{YZY}_{\boldsymbol{\theta},L}(x)$ can be represented in the form of a partial Fourier series with real coefficients.

Lemma 1 *There exists* $\boldsymbol{\theta} = (\theta_0, \theta_1, \ldots, \theta_L) \in \mathbb{R}^{L+1}$ *such that*

$$U^{YZY}_{\boldsymbol{\theta},L}(x) = \begin{bmatrix} P & -Q \\ Q^* & P^* \end{bmatrix} \tag{11}$$

if and only if real Laurent polynomials $P, Q \in \mathbb{R}[e^{ix/2}, e^{-ix/2}]$ *satisfy*

1. $\deg(P) = \deg(Q) \leq L$,
2. P *and* Q *have parity* $L \pmod 2$,
3. $\forall x \in \mathbb{R}$, $|P|^2 + |Q|^2 = 1$.

Lemma 1 decomposes the unitary matrix of the QNN $U^{YZY}_{\boldsymbol{\theta},L}(x)$ into Laurent polynomials with real coefficients, which can be used to represent a partial Fourier series with real coefficients. Note that the Fourier coefficients have a constraint $\sum_n |c_n| \leq 1$ by the condition 3 in Lemma 1.

The proof of Lemma 1 uses a method of mathematical induction that is in the similar spirit of the proof of quantum signal processing [32–34], which is a powerful subroutine in Hamiltonian simulation [4] and quantum singular value transformation [34]. The forward direction is straightforward by the definition of $U^{YZY}_{\boldsymbol{\theta},L}(x)$ in Eq. (10). The proof of the backward direction is by induction in L where the base case $L = 0$ holds trivially. For $L > 0$, we prove that for any $U^{YZY}_{\boldsymbol{\theta},L}(x)$ where P, Q satisfy the three conditions, there exists a unique block $R^\dagger_Y(\theta_k)R^\dagger_Z(x)$ such that polynomials $\hat{P}$ and $\hat{Q}$ in $U^{YZY}_{\boldsymbol{\theta},L}(x)R^\dagger_Y(\theta_k)R^\dagger_Z(x)$ satisfy the three conditions for $L-1$. Lemma 1 explicitly correlates the frequency spectrum of the Fourier series and the number of layers L of the QNN. Note that the proof of Lemma 1 also illustrates the exact correspondence between the Fourier coefficients and parameters of trainable gates. A detailed proof can be found in Appendix A.1.

By Lemma 1, the partial Fourier series corresponding to the QNN $U^{YZY}_{\boldsymbol{\theta},L}(x)$ only has real coefficients. With the exponential form of Eq. (6), a Fourier series with real coefficients only has $\cos(nx)$ terms, which means $U^{YZY}_{\boldsymbol{\theta},L}(x)$ can be used to approximate any even function on the interval $[-\pi, \pi]$. Thus we establish the following proposition, whose proof is deferred to Appendix A.2.

Proposition 2 *For any even square-integrable function* $f : [-\pi, \pi] \to [-1, 1]$ *and for all* $\epsilon > 0$, *there exists a QNN* $U^{YZY}_{\boldsymbol{\theta},L}(x)$ *such that* $|\psi(x)\rangle = U^{YZY}_{\boldsymbol{\theta},L}(x)\,|0\rangle$ *satisfies*

$$\| \langle\psi(x)|Z|\psi(x)\rangle - f(x)\| \leq \epsilon. \tag{12}$$

Although the above result states that the QNN $U^{YZY}_{\boldsymbol{\theta},L}(x)\,|0\rangle$ is able to approximate a class of even functions within arbitrary precision, we can see that the main limitation of the expressive power of QNN $U^{YZY}_{\boldsymbol{\theta},L}(x)$ is the real Fourier coefficients, which may restrict its universal approximation capability.

To tackle this issue, our idea is to introduce complex coefficients to the corresponding Laurent polynomials, which can be implemented by adding a trainable Pauli Z rotation operator in each layer. Specifically, we consider the QNN

$$U^{WZW}_{\boldsymbol{\theta},\boldsymbol{\phi},L}(x) = W(\theta_0, \phi_0) \prod_{j=1}^{L} R_Z(x) W(\theta_j, \phi_j), \tag{13}$$

where each trainable block is $W(\theta_j, \phi_j) \coloneqq R_Y(\theta_j)R_Z(\phi_j)$. The quantum circuit of $U^{WZW}_{\boldsymbol{\theta},\boldsymbol{\phi},L}(x)$ is illustrated in Fig. 3.

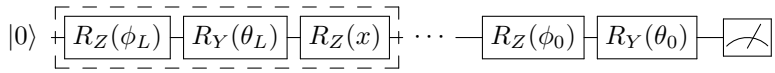

Figure 3: Circuit of $U^{WZW}_{\boldsymbol{\theta},\boldsymbol{\phi},L}(x)$, where the trainable block is composed of $R_Y(\cdot)$ and $R_Z(\cdot)$, and the encoding block is $R_Z(\cdot)$.

To characterize the capability of this QNN, we establish the following Lemma which implies $U^{WZW}_{\boldsymbol{\theta},\boldsymbol{\phi},L}(x)$ can express any Fourier partial sum with complex Fourier coefficients.

Lemma 3 *There exists* $\boldsymbol{\theta} = (\theta_0, \theta_1, \ldots, \theta_L) \in \mathbb{R}^{L+1}$ *and* $\boldsymbol{\phi} = (\phi_0, \phi_1, \ldots, \phi_L) \in \mathbb{R}^{L+1}$ *such that*

$$U^{WZW}_{\boldsymbol{\theta},\boldsymbol{\phi},L}(x) = \begin{bmatrix} P & -Q \\ Q^* & P^* \end{bmatrix} \tag{14}$$

if and only if Laurent polynomials $P, Q \in \mathbb{C}[e^{ix/2}, e^{-ix/2}]$ *satisfy*

1. $\deg(P) = \deg(Q) \leq L$,
2. P *and* Q *have parity* $L \pmod 2$,
3. $\forall x \in \mathbb{R}$, $|P|^2 + |Q|^2 = 1$.

Lemma 3 demonstrates a decomposition of the QNN $U^{WZW}_{\boldsymbol{\theta},\boldsymbol{\phi},L}(x)$ into Laurent polynomials with complex coefficients, which can be used to represent a partial Fourier series with complex coefficients in form of Eq. (8). The proof of Lemma 3 is similar to the proof of Lemma 1 and its details are provided in Appendix A.3. Again, the proof demonstrates the effect of parameterized gates on the control of Fourier coefficients. We then prove in the following Theorem 4 that $U^{WZW}_{\boldsymbol{\theta},\boldsymbol{\phi},L}(x)$ is able to approximate any square-integrable function within arbitrary precision, using the well-established result in Fourier analysis. The detailed proof is deferred to Appendix A.4.

Theorem 4 (Univariate approximation properties of single-qubit QNNs.) *For any univariate square-integrable function* $f : [-\pi, \pi] \to [-1, 1]$ *and for all* $\epsilon > 0$*, there exists a QNN* $U^{WZW}_{\boldsymbol{\theta},\boldsymbol{\phi},L}(x)$ *such that* $|\psi(x)\rangle = U^{WZW}_{\boldsymbol{\theta},\boldsymbol{\phi},L}(x)\,|0\rangle$ *satisfies*

$$\| \langle\psi(x)|Z|\psi(x)\rangle - f(x)\| \leq \epsilon. \tag{15}$$

Up till now we only let the encoding gate be the $R_Z(x)$ gate, what if we use other rotation operator gates to encode the data? It actually does not matter which one we choose as the encoding gate if the trainable gates are universal. Note that Pauli rotation operators $R_X(x), R_Y(x), R_Z(x)$ have two eigenvalues $\cos(x/2) \pm i\sin(x/2)$, and they can be diagonalized as $Q^\dagger R_Z(x) Q$. Merging unitaries $Q^\dagger$ and Q to universal trainable gates gives the QNN that uses $R_Z(x)$ as the encoding gate. We hereby define the generic single-qubit QNNs as

$$U^{UZU}_{\boldsymbol{\theta},\boldsymbol{\phi},\boldsymbol{\lambda},L}(x) = U_3(\theta_0, \phi_0, \lambda_0) \prod_{j=1}^{L} R_Z(x) U_3(\theta_j, \phi_j, \lambda_j), \tag{16}$$

where each trainable block is the generic rotation gate

$$U_3(\theta, \phi, \lambda) = \begin{bmatrix} \cos\frac{\theta}{2} & -e^{i\lambda}\sin\frac{\theta}{2} \\ e^{i\phi}\sin\frac{\theta}{2} & e^{i(\phi+\lambda)}\cos\frac{\theta}{2} \end{bmatrix}. \tag{17}$$

By definition, any L-layer single-qubit QNN, including $U^{WZW}_{\boldsymbol{\theta},\boldsymbol{\phi},L}$, can be expressed as $U^{UZU}_{\boldsymbol{\theta},\boldsymbol{\phi},\boldsymbol{\lambda},L}$. Thus $U^{UZU}_{\boldsymbol{\theta},\boldsymbol{\phi},\boldsymbol{\lambda},L}$ is surely a universal approximator.

4 Limitations of single-qubit QNNs

We have proved that a single-qubit QNN is a universal approximator for univariate functions, it is natural to consider its limitations. Is there a single-qubit QNN that can approximate arbitrary multivariate functions? We answer this question from the perspective of multivariate Fourier series.

Specifically, we consider the generic form of single-qubit QNNs defined in Eq. (16) and upload the classical data $\boldsymbol{x} := (x^{(1)}, x^{(2)}, \cdots, x^{(d)}) \in \mathbb{R}^d$ as

$$U_{\boldsymbol{\theta},L}(\boldsymbol{x}) = U_3(\theta_0, \phi_0, \lambda_0) \prod_{j=1}^{L} R_Z(x_j) U_3(\theta_j, \phi_j, \lambda_j), \tag{18}$$

where each $x_j \in \boldsymbol{x}$ and $L \in \mathbb{N}^+$. Without loss of generality, assume that each dimension $x^{(i)}$ is uploaded the same number of times, denoted by K. Naturally, we have $Kd = L$. Further, we rewrite the output of QNNs defined in Eq. (5) as the following form.

$$f_{\boldsymbol{\theta},L}(\boldsymbol{x}) = \sum_{\boldsymbol{\omega} \in \Omega} c_{\boldsymbol{\omega}} e^{i\boldsymbol{\omega}\cdot\boldsymbol{x}}, \tag{19}$$

where $\Omega = \{-K, \cdots, 0, \cdots, K\}^d$, and the $c_{\boldsymbol{\omega}}$ is determined by parameters $\boldsymbol{\theta}$ and the observable M. A detailed analysis can be found in Appendix B. We can see that Eq. (19) cannot be represented as a K-truncated multivariate Fourier series. Specifically, by the curse of dimensionality, it requires exponentially many terms in d to approximate a function in d dimensions. However, for $f_{\boldsymbol{\theta},L}(\boldsymbol{x})$, the degrees of freedom grow linearly with the number of layers L. It implies that single-qubit native QNNs potentially lack the capability to universally approximate arbitrary multivariate functions from the perspective of the Fourier series.

Despite the potential limitation of native QNNs in multivariate approximation, it has been proved that a single-qubit **hybrid** QNN can approximate arbitrary multivariate functions [28, 29]. However, the UAP of hybrid QNNs is fundamentally different from the native model that we investigated. Those hybrid models involve trainable weights either in data pre-processing or post-processing. Specifically, introducing trainable weights in data pre-processing is equivalent to multiplying each frequency of the Fourier series by an arbitrary real coefficient, i.e.

$$S(wx) = R_Z(wx) = e^{-iw\frac{x}{2}Z}. \tag{20}$$

Therefore it enriches the frequency spectrum of native QNNs, which only contain integer multiples of the fundamental frequency. It can also be readily extended to the encoding of multi-dimensional data $\boldsymbol{x} := (x^{(1)}, x^{(2)}, \cdots, x^{(d)})$ as

$$R_Z(w_1 x^{(1)}) R_Z(w_2 x^{(2)}) \cdots R_Z(w_d x^{(d)}) = R_Z(\boldsymbol{w} \cdot \boldsymbol{x}) = e^{-\frac{1}{2} i \boldsymbol{w}\cdot\boldsymbol{x} Z}, \tag{21}$$

where $\boldsymbol{w} = (w_1, \ldots, w_d)$ is a vector of trainable weights. Using such an encoding method enables a single-qubit QNN to approximate any continuous multivariate function [29]. We notice that, although the trainable weights enrich the frequency spectrum of the Fourier series, the capability of hybrid QNNs to approximate arbitrary multivariate functions is not obtained using the multivariate Fourier series, but the universal approximation theorem [25, 26] in machine learning theory. In another word, the multivariate UAP of a hybrid QNN mostly comes from the classical structure, and the QNN serves as an activation function $\sigma(x) = e^{-ix}$ in the universal approximation theorem. This fact might be able to shed some light on the reason why a hybrid QNN does not provide quantum advantages over the classical NN.

5 Numerical experiments

In order to better illustrate the expressive power of single-qubit native QNNs, we supplement the theoretical results with numerical experiments. Specifically, we demonstrate the flexibility and approximation capability of single-qubit native QNNs in Section 5.1. The limitations of single-qubit QNNs are illustrated in Section 5.2 through the numerical experiments on approximating multivariate functions. All simulations are carried out with the Paddle Quantum toolkit on the PaddlePaddle Deep Learning Platform, using a desktop with an 8-core i7 CPU and 32GB RAM.

5.1 Univariate function approximation

A damping function $f(x) = \frac{\sin(5x)}{5x}$ is used to demonstrate the approximation performance of single-qubit native QNN models. The dataset consists of 300 data points uniformly sampled from the interval $[0, \pi]$, from which 200 are selected for the training set and 100 for the test set. Since the

function $f(x)$ is an even function, we use the QNN model as defined in Eq. (10). The parameters of trainable gates are initialized from the uniform distribution on $[0, 2\pi]$. We adopt a variational quantum algorithm, where a gradient-based optimizer is used to search and update parameters in the QNN. The mean squared error (MSE) serves as the loss function. Here the Adam optimizer is used with a learning rate of 0.1. We set the training iterations to be 100 with a batch size of 20 for all experiments.

While approximating a function $f(x)$ by a truncated Fourier series, the approximation error decreases as the number of expansion terms increases. As shown in Lemma 3, the frequency spectrum and Fourier coefficients will be extended by consecutive repetitions of the encoding gate and trainable gate. The numerical results in Fig. 4 illustrate that the approximation error decreases as the number of layers increases, which are consistent with our theoretical analysis.

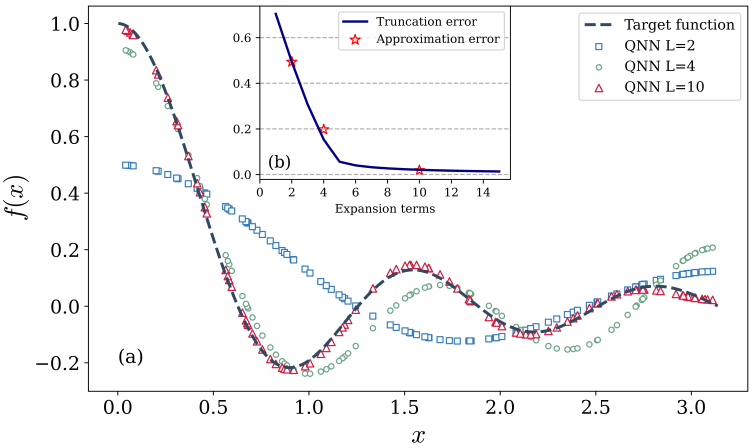

Figure 4: Panel (a) is the approximation results of $U^{YZY}_{\boldsymbol{\theta},L}$ with different L. Panel (b) shows the approximation error. Here the theoretical truncation error is calculated using the uniform norm $\|f_N(x) - f(x)\|_\infty$, where $f_N(x)$ is the truncated Fourier series of $f(x)$ with N terms.

To further show the flexibility and capability of single-qubit QNNs, we pick a square wave function as the target function. The training set contains 400 data points sampled from the interval $[0, 20]$. The numerical results are illustrated in Fig. 5. By simply repeating 45 layers, the single-qubit QNN $U^{WZW}_{\boldsymbol{\theta},\boldsymbol{\phi},L}(x)$ learns the function hidden beneath the training data. In particular, the approximation works well not only for input variables located between the training data but also outside of the region, because the Fourier series has a natural capability in dealing with periodic functions.

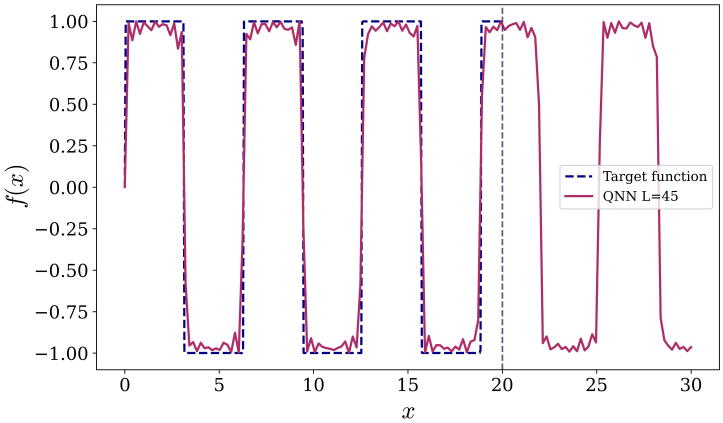

Figure 5: The result of approximating the square wave function by a 45-layer QNN $U^{WZW}_{\boldsymbol{\theta},\boldsymbol{\phi},L}(x)$. For showing periodic extrapolation, and the test region is extend to $[0, 30]$.

5.2 Multivariate function approximation

We numerically demonstrate the limitations of single-qubit native QNNs in approximate multivariate functions. We examine the convergence of the loss as the number of layers of the circuit increases and compare the outcome with the target function. Specifically, we consider a bivariate function $f(x, y) = (x^2 + y - 1.5\pi)^2 + (x + y^2 - \pi)^2$ as the target function. Note that $f(x, y)$ is normalized on the interval $[-\pi, \pi]^2$, i.e., $-1 \leq f(x, y) \leq 1$.

The training set consists of 400 data points sampled from interval $[-\pi, \pi]^2$. We use the single-qubit QNN with various numbers of layers defined as Eq. (18) to learn the target function. The experimental setting is the same as in the univariate function approximation. In order to reduce the effect of randomness, the experimental results are averaged over 5 independent training instances.

Fig. 6 shows that the single-qubit native QNN has difficulty in approximating bivariate functions. The approximation result of QNN as shown in Fig. 6b is quite different from the target function, even for a very deep circuit of 40 layers. Also, the training loss in Fig. 6c does not decrease as the number of layers increases. Note that the target function is only bivariate here, the limitations of single-qubit native QNNs will be more obvious in the case of higher dimensions. We further propose a possible strategy that extends single-qubit QNNs to multiple qubits, which could potentially overcome the limitations and handle practical classification tasks, see Appendix C for details.

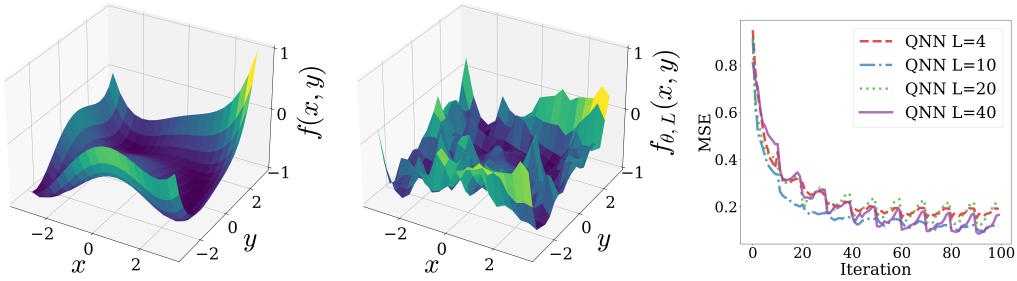

(a) Target function. (b) Approximation result. (c) Training loss.

Figure 6: Panel (a) is the plot of target function $f(x, y)$. Panel (b) shows the approximation result of a 40-layer QNN. Panel (c) is the plot of training loss for QNNs with different numbers of layers during the optimization.

6 Conclusion and outlook

In this work, we presented a systematic investigation of the expressive power of single-qubit native QNNs, which are capable to approximate any square-integrable univariate function with arbitrary precision. We not only give an existence proof but also analytically show an exact mapping between native QNNs and the partial Fourier series from perspectives of both frequency spectrum and Fourier coefficients, which solves an open problem on the UAP of single-qubit QNNs in Ref. [27]. Our proof, inspired by quantum signal processing, explicitly illustrates the correlation between parameters of trainable gates and the Fourier coefficients. Other than the expressivity, we also discuss the limitation of single-qubit QNNs from the perspective of multivariate Fourier series. Both the expressivity and limitation of single-qubit QNNs are validated by numerical simulations. We expect our results provide a fundamental framework to the class of data re-uploading QNNs, which serves as insightful guidance on the design of such QNN models.

Although the expressive power of a single-qubit QNN have been well investigated, it may not be an ideal model in practice due to the potential limitations on approximating multivariate functions. Moreover, single-qubit models can be efficiently simulated by classical computers and hence cannot bring any quantum advantage. Therefore one future step is to generalize the framework of single-qubit QNNs to multivariate function approximators. The multi-qubit QNNs with UAP as shown in Ref. [27] require exponential circuit depth, which is impractical to implement and also does not imply quantum advantage. It is of great interest to investigate the efficient implementation of QNNs with universal approximation properties for multivariate functions. A recent paper presents a method that extends quantum signal processing to multivariable [35], which might be applicable to single-qubit QNNs.

References

[1] Peter W. Shor. Polynomial-Time Algorithms for Prime Factorization and Discrete Logarithms on a Quantum Computer. *SIAM Journal on Computing*, 26(5):1484–1509, oct 1997. ISSN 0097-5397. doi: 10.1137/S0097539795293172. URL http://epubs.siam.org/doi/10.1137/S0097539795293172.

[2] Lov K Grover. A fast quantum mechanical algorithm for database search. In *Proceedings of the twenty-eighth annual ACM symposium on Theory of computing - STOC '96*, pages 212–219, New York, New York, USA, 1996. ACM Press. ISBN 0897917855. doi: 10.1145/237814.237866. URL http://portal.acm.org/citation.cfm?doid=237814.237866.

[3] Seth Lloyd. Universal Quantum Simulators. *Science*, 273(5278):1073–1078, aug 1996. ISSN 0036-8075. doi: 10.1126/science.273.5278.1073. URL http://www.sciencemag.org/cgi/doi/10.1126/science.273.5278.1073.

[4] Andrew M. Childs, Dmitri Maslov, Yunseong Nam, Neil J. Ross, and Yuan Su. Toward the first quantum simulation with quantum speedup. *Proceedings of the National Academy of Sciences*, 115(38):9456–9461, sep 2018. ISSN 0027-8424. doi: 10.1073/pnas.1801723115. URL http://arxiv.org/abs/1711.10980http://www.pnas.org/lookup/doi/10.1073/pnas.1801723115.

[5] Frank Arute, Kunal Arya, Ryan Babbush, Dave Bacon, Joseph C Bardin, Rami Barends, Rupak Biswas, Sergio Boixo, Fernando GSL Brandao, David A Buell, et al. Quantum supremacy using a programmable superconducting processor. *Nature*, 574(7779):505–510, 2019.

[6] Yulin Wu, Wan-Su Bao, Sirui Cao, Fusheng Chen, Ming-Cheng Chen, Xiawei Chen, Tung-Hsun Chung, Hui Deng, Yajie Du, Daojin Fan, Ming Gong, Cheng Guo, Chu Guo, Shaojun Guo, Lianchen Han, Linyin Hong, He-Liang Huang, Yong-Heng Huo, Liping Li, Na Li, Shaowei Li, Yuan Li, Futian Liang, Chun Lin, Jin Lin, Haoran Qian, Dan Qiao, Hao Rong, Hong Su, Lihua Sun, Liangyuan Wang, Shiyu Wang, Dachao Wu, Yu Xu, Kai Yan, Weifeng Yang, Yang Yang, Yangsen Ye, Jianghan Yin, Chong Ying, Jiale Yu, Chen Zha, Cha Zhang, Haibin Zhang, Kaili Zhang, Yiming Zhang, Han Zhao, Youwei Zhao, Liang Zhou, Qingling Zhu, Chao-Yang Lu, Cheng-Zhi Peng, Xiaobo Zhu, and Jian-Wei Pan. Strong Quantum Computational Advantage Using a Superconducting Quantum Processor. *Physical Review Letters*, 127(18):180501, oct 2021. ISSN 0031-9007. doi: 10.1103/PhysRevLett.127.180501. URL https://link.aps.org/doi/10.1103/PhysRevLett.127.180501.

[7] Han-Sen Zhong, Hui Wang, Yu-Hao Deng, Ming-Cheng Chen, Li-Chao Peng, Yi-Han Luo, Jian Qin, Dian Wu, Xing Ding, Yi Hu, Peng Hu, Xiao-Yan Yang, Wei-Jun Zhang, Hao Li, Yuxuan Li, Xiao Jiang, Lin Gan, Guangwen Yang, Lixing You, Zhen Wang, Li Li, Nai-Le Liu, Chao-Yang Lu, and Jian-Wei Pan. Quantum computational advantage using photons. *Science*, 370(6523):1460–1463, dec 2020. ISSN 0036-8075. doi: 10.1126/science.abe8770. URL https://www.science.org/doi/10.1126/science.abe8770.

[8] Jacob Biamonte, Peter Wittek, Nicola Pancotti, Patrick Rebentrost, Nathan Wiebe, and Seth Lloyd. Quantum machine learning. *Nature*, 549(7671):195–202, sep 2017. ISSN 0028-0836. doi: 10.1038/nature23474. URL http://dx.doi.org/10.1038/nature23474http://www.nature.com/articles/nature23474.

[9] M. Cerezo, Andrew Arrasmith, Ryan Babbush, Simon C. Benjamin, Suguru Endo, Keisuke Fujii, Jarrod R. McClean, Kosuke Mitarai, Xiao Yuan, Lukasz Cincio, and Patrick J. Coles. Variational quantum algorithms. *Nature Reviews Physics*, aug 2021. ISSN 2522-5820. doi: 10.1038/s42254-021-00348-9. URL https://www.nature.com/articles/s42254-021-00348-9.

[10] Kishor Bharti, Alba Cervera-Lierta, Thi Ha Kyaw, Tobias Haug, Sumner Alperin-Lea, Abhinav Anand, Matthias Degroote, Hermanni Heimonen, Jakob S Kottmann, Tim Menke, Wai-Keong Mok, Sukin Sim, Leong-Chuan Kwek, and Alán Aspuru-Guzik. Noisy intermediate-scale quantum (NISQ) algorithms. *arXiv:2101.08448*, pages 1–82, jan 2021. URL http://arxiv.org/abs/2101.08448.

[11] Suguru Endo, Zhenyu Cai, Simon C Benjamin, and Xiao Yuan. Hybrid Quantum-Classical Algorithms and Quantum Error Mitigation. *Journal of the Physical Society of Japan*, 90(3):032001, mar 2021. ISSN 0031-9015. doi: 10.7566/JPSJ.90.032001. URL http://arxiv.org/abs/2011.01382https://journals.jps.jp/doi/10.7566/JPSJ.90.032001.

[12] Jonathan Romero, Jonathan P. Olson, and Alan Aspuru-Guzik. Quantum autoencoders for efficient compression of quantum data. *Quantum Science and Technology*, 2(4):045001, dec 2017. ISSN 2058-9565. doi: 10.1088/2058-9565/aa8072. URL http://stacks.iop.org/2058-9565/2/i=4/a=045001?key=crossref.03b058bfdad4fe46f9a2bc5ffae3961e.

[13] Chenfeng Cao and Xin Wang. Noise-Assisted Quantum Autoencoder. *Physical Review Applied*, 15(5):054012, may 2021. ISSN 2331-7019. doi: 10.1103/PhysRevApplied.15.054012. URL http://arxiv.org/abs/2012.08331https://link.aps.org/doi/10.1103/PhysRevApplied.15.054012.

[14] Iris Cong, Soonwon Choi, and Mikhail D. Lukin. Quantum convolutional neural networks. *Nature Physics*, 15(12):1273–1278, dec 2019. ISSN 1745-2473. doi: 10.1038/s41567-019-0648-8. URL http://arxiv.org/abs/1810.03787http://www.nature.com/articles/s41567-019-0648-8.

[15] Weikang Li and Dong-Ling Deng. Recent advances for quantum classifiers. *arXiv:2108.13421*, aug 2021. URL http://arxiv.org/abs/2108.13421.

[16] Maria Schuld and Francesco Petruccione. *Machine Learning with Quantum Computers*. Springer, 2021.

[17] G. Li, Z. Song, and X. Wang. VSQL: Variational shadow quantum learning for classification. In *Proceedings of the AAAI Conference on Artificial Intelligence, 35(9), 8357-8365*, 2021.

[18] Sumeet Khatri, Ryan LaRose, Alexander Poremba, Lukasz Cincio, Andrew T. Sornborger, and Patrick J. Coles. Quantum-assisted quantum compiling. *Quantum*, 3:140, jul 2018. ISSN 2521-327X. doi: 10.22331/q-2019-05-13-140. URL https://quantum-journal.org/papers/q-2019-05-13-140/http://arxiv.org/abs/1807.00800http://dx.doi.org/10.22331/q-2019-05-13-140.

[19] Zhan Yu, Xuanqiang Zhao, Benchi Zhao, and Xin Wang. Optimal quantum dataset for learning a unitary transformation. *arXiv preprint arXiv:2203.00546*, mar 2022. URL http://arxiv.org/abs/2203.00546.

[20] Matthias C Caro, Hsin-Yuan Huang, Nicholas Ezzell, Joe Gibbs, Andrew T Sornborger, Lukasz Cincio, Patrick J Coles, and Zoë Holmes. Out-of-distribution generalization for learning quantum dynamics. *arXiv preprint arXiv:2204.10268*, apr 2022. URL http://arxiv.org/abs/2204.10268.

[21] Sam McArdle, Suguru Endo, Alán Aspuru-Guzik, Simon C. Benjamin, and Xiao Yuan. Quantum computational chemistry. *Reviews of Modern Physics*, 92(1):015003, mar 2020. ISSN 0034-6861. doi: 10.1103/RevModPhys.92.015003. URL https://link.aps.org/doi/10.1103/RevModPhys.92.015003.

[22] Bálint Koczor, Suguru Endo, Tyson Jones, Yuichiro Matsuzaki, and Simon C Benjamin. Variational-state quantum metrology. *New Journal of Physics*, 22(8):083038, aug 2020. ISSN 1367-2630. doi: 10.1088/1367-2630/ab965e. URL https://iopscience.iop.org/article/10.1088/1367-2630/ab965e.

[23] Jacob L. Beckey, M. Cerezo, Akira Sone, and Patrick J. Coles. Variational quantum algorithm for estimating the quantum Fisher information. *Physical Review Research*, 4(1):013083, feb 2022. ISSN 2643-1564. doi: 10.1103/PhysRevResearch.4.013083. URL https://link.aps.org/doi/10.1103/PhysRevResearch.4.013083.

[24] Johannes Jakob Meyer, Johannes Borregaard, and Jens Eisert. A variational toolbox for quantum multi-parameter estimation. *npj Quantum Information*, 7(1): 89, dec 2021. ISSN 2056-6387. doi: 10.1038/s41534-021-00425-y. URL http://dx.doi.org/10.1038/s41534-021-00425-yhttp://www.nature.com/articles/s41534-021-00425-y.

[25] George Cybenko. Approximation by superpositions of a sigmoidal function. *Mathematics of control, signals and systems*, 2(4):303–314, 1989. URL https://link.springer.com/article/10.1007/BF02551274.

[26] Kurt Hornik. Approximation capabilities of multilayer feedforward networks. *Neural networks*, 4(2):251–257, 1991. URL https://www.sciencedirect.com/science/article/abs/pii/089360809190009T.

[27] Maria Schuld, Ryan Sweke, and Johannes Jakob Meyer. Effect of data encoding on the expressive power of variational quantum-machine-learning models. *Physical Review A*, 103(3): 032430, 2021. URL https://doi.org/10.1103/PhysRevA.103.032430.

[28] Takahiro Goto, Quoc Hoan Tran, and Kohei Nakajima. Universal approximation property of quantum machine learning models in quantum-enhanced feature spaces. *Physical Review Letters*, 127(9):090506, 2021. URL https://journals.aps.org/prl/abstract/10.1103/PhysRevLett.127.090506.

[29] Adrián Pérez-Salinas, David López-Núñez, Artur García-Sáez, Pol Forn-Díaz, and José I Latorre. One qubit as a universal approximant. *Physical Review A*, 104(1):012405, 2021. URL https://journals.aps.org/pra/abstract/10.1103/PhysRevA.104.012405.

[30] Adrián Pérez-Salinas, Alba Cervera-Lierta, Elies Gil-Fuster, and José I. Latorre. Data re-uploading for a universal quantum classifier. *Quantum*, 4:226, February 2020. doi: 10.22331/q-2020-02-06-226.

[31] Sofiene Jerbi, Lukas J. Fiderer, Hendrik Poulsen Nautrup, Jonas M. Kübler, Hans J. Briegel, and Vedran Dunjko. Quantum machine learning beyond kernel methods. *arXiv:2110.13162 [quant-ph, stat]*, February 2022.

[32] Guang Hao Low and Isaac L. Chuang. Optimal hamiltonian simulation by quantum signal processing. *Physical Review Letters*, 118(1):010501, January 2017. doi: 10.1103/PhysRevLett.118.010501.

[33] Jeongwan Haah. Product decomposition of periodic functions in quantum signal processing. *Quantum*, 3:190, October 2019. ISSN 2521-327X. doi: 10.22331/q-2019-10-07-190.

[34] András Gilyén, Yuan Su, Guang Hao Low, and Nathan Wiebe. Quantum singular value transformation and beyond: Exponential improvements for quantum matrix arithmetics. *Proceedings of the 51st Annual ACM SIGACT Symposium on Theory of Computing*, pages 193–204, June 2019. doi: 10.1145/3313276.3316366.

[35] Zane M. Rossi and Isaac L. Chuang. Multivariable quantum signal processing (m-qsp): Prophecies of the two-headed oracle. (arXiv:2205.06261), May 2022.

[36] Ferenc Weisz. Summability of multi-dimensional trigonometric fourier series. *arXiv preprint arXiv:1206.1789*, 2012.

[37] Jun Zhang, Jiri Vala, Shankar Sastry, and K. Birgitta Whaley. Exact Two-Qubit Universal Quantum Circuit. *Physical Review Letters*, 91(2):027903, July 2003. doi: 10.1103/PhysRevLett.91.027903.

[38] G. Vidal and C. M. Dawson. Universal quantum circuit for two-qubit transformations with three controlled-NOT gates. *Physical Review A*, 69(1):010301, January 2004. doi: 10.1103/PhysRevA.69.010301.

[39] Ronald A Fisher. The use of multiple measurements in taxonomic problems. *Annals of eugenics*, 7(2):179–188, 1936.

[40] Ryszard S Michalski, Igor Mozetic, Jiarong Hong, and Nada Lavrac. The multi-purpose incremental learning system aq15 and its testing application to three medical domains. In *Proc. AAAI*, volume 1986, pages 1–041, 1986.

[41] Robert J Lyon, BW Stappers, Sally Cooper, John Martin Brooke, and Joshua D Knowles. Fifty years of pulsar candidate selection: from simple filters to a new principled real-time classification approach. *Monthly Notices of the Royal Astronomical Society*, 459(1):1104–1123, 2016.

Checklist

1. For all authors...
   (a) Do the main claims made in the abstract and introduction accurately reflect the paper's contributions and scope? [Yes]
   (b) Did you describe the limitations of your work? [Yes] See Section 4 and Section 5.2.
   (c) Did you discuss any potential negative societal impacts of your work? [No]
   (d) Have you read the ethics review guidelines and ensured that your paper conforms to them? [Yes]
2. If you are including theoretical results...
   (a) Did you state the full set of assumptions of all theoretical results? [Yes]
   (b) Did you include complete proofs of all theoretical results? [Yes] See Appendix A.
3. If you ran experiments...
   (a) Did you include the code, data, and instructions needed to reproduce the main experimental results (either in the supplemental material or as a URL)? [Yes]
   (b) Did you specify all the training details (e.g., data splits, hyperparameters, how they were chosen)? [Yes] See Section 5.
   (c) Did you report error bars (e.g., with respect to the random seed after running experiments multiple times)? [No]
   (d) Did you include the total amount of compute and the type of resources used (e.g., type of GPUs, internal cluster, or cloud provider)? [Yes] See Section 5.
4. If you are using existing assets (e.g., code, data, models) or curating/releasing new assets...
   (a) If your work uses existing assets, did you cite the creators? [Yes] See Appendix C.
   (b) Did you mention the license of the assets? [Yes] See Appendix C.
   (c) Did you include any new assets either in the supplemental material or as a URL? [N/A]
   (d) Did you discuss whether and how consent was obtained from people whose data you're using/curating? [N/A]
   (e) Did you discuss whether the data you are using/curating contains personally identifiable information or offensive content? [N/A]
5. If you used crowdsourcing or conducted research with human subjects...
   (a) Did you include the full text of instructions given to participants and screenshots, if applicable? [N/A]
   (b) Did you describe any potential participant risks, with links to Institutional Review Board (IRB) approvals, if applicable? [N/A]
   (c) Did you include the estimated hourly wage paid to participants and the total amount spent on participant compensation? [N/A]

Appendix for Power and limitations of single-qubit native quantum neural networks

A Detailed Proofs

A.1 Proof of Lemma 1

Lemma 1 *There exists* $\boldsymbol{\theta} = (\theta_0, \theta_1, \ldots, \theta_L) \in \mathbb{R}^{L+1}$ *such that*

$$U^{YZY}_{\boldsymbol{\theta},L}(x) = \begin{bmatrix} P & -Q \\ Q^* & P^* \end{bmatrix} \tag{S1}$$

if and only if real Laurent polynomials $P, Q \in \mathbb{R}[e^{ix/2}, e^{-ix/2}]$ *satisfy*

1. $\deg(P) = \deg(Q) \leq L$,
2. P *and* Q *have parity* $L \pmod 2$,
3. $\forall x \in \mathbb{R}$, $|P|^2 + |Q|^2 = 1$.

Proof First we prove the forward direction, i.e. Eq. (S1) implies the three conditions, by induction on L. For the base case, if $L = 0$, then $R_Y(\theta_0)$ gives $P = \cos(\theta_0/2)$ and $Q = \sin(\theta_0/2)$, which clearly satisfies the conditions.

For the induction step, suppose Eq. (S1) satisfies the three conditions. Then

$$\begin{bmatrix} P & -Q \\ Q^* & P^* \end{bmatrix} R_Z(x) R_Y(\theta_k) \tag{S2}$$

$$= \begin{bmatrix} P & -Q \\ Q^* & P^* \end{bmatrix} \begin{bmatrix} \cos(\theta_k/2)e^{-ix/2} & -\sin(\theta_k/2)e^{-ix/2} \\ \sin(\theta_k/2)e^{ix/2} & \cos(\theta_k/2)e^{ix/2} \end{bmatrix} \tag{S3}$$

$$= \begin{bmatrix} \cos\frac{\theta_k}{2}e^{-ix/2}P - \sin\frac{\theta_k}{2}e^{ix/2}Q & -\sin\frac{\theta_k}{2}e^{-ix/2}P - \cos\frac{\theta_k}{2}e^{ix/2}Q \\ \cos\frac{\theta_k}{2}e^{-ix/2}Q^* + \sin\frac{\theta_k}{2}e^{ix/2}P^* & \cos\frac{\theta_k}{2}e^{ix/2}P^* - \sin\frac{\theta_k}{2}e^{-ix/2}Q^* \end{bmatrix} \tag{S4}$$

$$= \begin{bmatrix} \bar{P} & -\bar{Q} \\ \bar{Q}^* & \bar{P}^* \end{bmatrix} \tag{S5}$$

where

$$\bar{P} = \cos\frac{\theta_k}{2}e^{-ix/2}P - \sin\frac{\theta_k}{2}e^{ix/2}Q, \tag{S6}$$

$$\bar{Q} = \sin\frac{\theta_k}{2}e^{-ix/2}P + \cos\frac{\theta_k}{2}e^{ix/2}Q \tag{S7}$$

clearly satisfy the first condition $\deg(\bar{P}) = \deg(\bar{Q}) \leq L + 1$. They also satisfy the second condition since multiplying by $e^{-ix/2}$ or $e^{ix/2}$ alters the parity. The third condition follows from unitarity.

Next we show the reverse by induction on L that the three conditions suffice to construct the QNN in Eq. (S1). For the base case, we have $L = 0$ and $\deg(P) = \deg(Q) = 0$. Note that P and Q are real polynomials, i.e. the coefficients must be real numbers, so condition 3 implies that $P = \cos(\theta_0/2)$ and $Q = \sin(\theta_0/2)$ for some $\theta_0 \in \mathbb{R}$. Thus the matrix

$$\begin{bmatrix} P & -Q, \\ Q^* & P^* \end{bmatrix} \tag{S8}$$

can be written as a QNN $U^{YZY}_{\boldsymbol{\theta},0}(x) = R_Y(\theta_0)$.

For the induction step, suppose Laurent polynomials P and Q satisfy the three conditions for some $L > 0$. We first observe that condition 3 implies

$$|P|^2 + |Q|^2 = PP^* + QQ^* = 1, \tag{S9}$$

where $PP^* + QQ^*$ is a Laurent polynomial with parity $2n \pmod 2 \equiv 0$. Let $d \coloneqq \deg(P) = \deg(Q)$, then $d \leq L$ by the first condition. Since Eq. (S9) holds for all $x \in \mathbb{R}$, the leading coefficients

must satisfy $p_d p_{-d} + q_d q_{-d} = 0$ so they cancel. We choose $\theta_k \in \mathbb{R}$ so that

$$\cos\frac{\theta_k}{2} p_d + \sin\frac{\theta_k}{2} q_d = 0, \tag{S10}$$

$$-\sin\frac{\theta_k}{2} p_{-d} + \cos\frac{\theta_k}{2} q_{-d} = 0. \tag{S11}$$

Now we briefly argue that there always exists a θ_k satisfies equations above. If all p_d, p_{-d}, q_d, q_{-d} are not 0, simply let $\tan\frac{\theta_k}{2} = -\frac{p_d}{q_d}$. Then consider the case of zero coefficients. Since $\deg(P) = \deg(Q) = d$, at most two of p_d, p_{-d}, q_d, q_{-d} could be 0. The fact $p_d p_{-d} + q_d q_{-d} = 0$ implies that one of p_d, p_{-d} is 0 if and only if one of q_d, q_{-d} is 0. If $p_d = q_d = 0$ (or $p_{-d} = q_{-d} = 0$), pick θ_k so that $\tan\frac{\theta_k}{2} = \frac{q_{-d}}{p_{-d}}$ (or $\tan\frac{\theta_k}{2} = -\frac{p_d}{q_d}$). If $p_d = q_{-d} = 0$ (or $p_{-d} = q_d = 0$), pick θ_k so that $\sin\frac{\theta_k}{2} = 0$ (or $\cos\frac{\theta_k}{2} = 0$).

Next, for the θ_k that satisfies Eq. (S10) and Eq. (S11) simultaneously, we consider

$$\begin{bmatrix} P & -Q \\ Q^* & P^* \end{bmatrix} R_Y^\dagger(\theta_k) R_Z^\dagger(x) \tag{S12}$$

$$= \begin{bmatrix} \cos\frac{\theta_k}{2} e^{ix/2} P + \sin\frac{\theta_k}{2} e^{ix/2} Q & -\cos\frac{\theta_k}{2} e^{-ix/2} Q + \sin\frac{\theta_k}{2} e^{-ix/2} P \\ \cos\frac{\theta_k}{2} e^{ix/2} Q^* - \sin\frac{\theta_k}{2} e^{ix/2} P^* & \cos\frac{\theta_k}{2} e^{-ix/2} P^* + \sin\frac{\theta_k}{2} e^{-ix/2} Q \end{bmatrix} \tag{S13}$$

$$= \begin{bmatrix} \hat{P} & -\hat{Q} \\ \hat{Q}^* & \hat{P}^* \end{bmatrix} \tag{S14}$$

where

$$\hat{P} = \cos\frac{\theta_k}{2} e^{ix/2} P + \sin\frac{\theta_k}{2} e^{ix/2} Q, \tag{S15}$$

$$\hat{Q} = \cos\frac{\theta_k}{2} e^{-ix/2} Q - \sin\frac{\theta_k}{2} e^{-ix/2} P. \tag{S16}$$

Since $P, Q \in \mathbb{R}[e^{ix/2}, e^{-ix/2}]$ are Laurent polynomials with degree d, $\hat{P} \in \mathbb{R}[e^{ix/2}, e^{-ix/2}]$ might appear to be a Laurent polynomial with degree $d+1$. In fact it has degree $\deg(\hat{P}) \leq d-1$, because the coefficient of $(e^{ix/2})^{d+1}$ term in $\hat{P}$ is $\cos\frac{\theta_k}{2} p_d + \sin\frac{\theta_k}{2} q_d = 0$ by the choice of θ_k, and the coefficient of $(e^{ix/2})^d$ term is 0 by condition 2. Similarly, $\hat{Q}$ has leading coefficient $\cos\frac{\theta_k}{2} q_{-d} - \sin\frac{\theta_k}{2} p_{-d} = 0$ and has degree $\deg(\hat{Q}) \leq d-1$. Since $d \leq L$, we have $\deg(\hat{P}) = \deg(\hat{Q}) \leq L-1$, hence condition 1 is satisfied. From the parity of P and Q, it is easy to see that $\hat{P}$ and $\hat{Q}$ have parity $L-1 \pmod 2$, thus condition 2 is satisfied. Condition 3 follows from unitarity. By the induction hypothesis, Eq. (S14) can be written as a QNN in the form of $U^{YZY}_{\boldsymbol{\theta},L-1}(x)$, and therefore the matrix

$$\begin{bmatrix} P & -Q \\ Q^* & P^* \end{bmatrix} \tag{S17}$$

can be written as a QNN in the form of $U^{YZY}_{\boldsymbol{\theta},L}(x)$. ■

We note that the above proof is in a similar spirit of the proof of quantum signal processing [32–34].

A.2 Proof of Proposition 2

Proposition 2 *For any even square-integrable function $f : [-\pi, \pi] \to [-1, 1]$ and for all $\epsilon > 0$, there exists a QNN $U^{YZY}_{\boldsymbol{\theta},L}(x)$ such that $|\psi(x)\rangle = U^{YZY}_{\boldsymbol{\theta},L}(x)\,|0\rangle$ satisfies*

$$\|\langle\psi(x)|Z|\psi(x)\rangle - f(x)\| \leq \epsilon. \tag{S18}$$

Proof First, it is known that any even square-integrable function $f(x)$ can be approximated by a truncated Fourier series [36]. For any $\epsilon > 0$, there exists a $K \in \mathbb{N}^+$ such that

$$\|f_K(x) - f(x)\| \leq \frac{\epsilon}{2}, \tag{S19}$$

where $f_K(x)$ is the K-term partial Fourier series of even function $f(x)$. Consider the function $\sqrt{\frac{1+f_K(x)}{2}}$, using the property of square-integrable functions again, there exists an $L \in \mathbb{N}^+$ such that

$$\left\| g_L(x) - \sqrt{\frac{1+f_K(x)}{2}} \right\| \leq \frac{\epsilon}{8}, \tag{S20}$$

where

$$g_L(x) = a_0 + \sum_{n=1}^{L/2} a_n \cos(nx) \tag{S21}$$

is the partial Fourier series of the even function $\sqrt{\frac{1+f_K(x)}{2}}$ and $L \pmod 2 = 0$. Next we need to prove

$$\langle 0 | U^{YZY}_{\boldsymbol{\theta},L}(x) | 0 \rangle = g_L(x). \tag{S22}$$

Specifically, $g_L(x)$ can be written as follows,

$$g_L(x) = \sum_{n=-L/2}^{L/2} c_n e^{inx} = \sum_{n=-L/2}^{L/2} c_n (e^{ix/2})^{2n}, \tag{S23}$$

where $c_n = c_{-n} = a_n/2$. Obviously, $g_L \in \mathbb{R}[e^{ix/2}, e^{-ix/2}]$ and conditions of Lemma 1 are satisfied, so Eq. (S22) holds. Further, we have

$$\begin{aligned} \| \langle \psi(x) | Z | \psi(x) \rangle - f_K(x) \| &= 2 \left\| g_L^2(x) - \frac{1+f_K(x)}{2} \right\|, & \text{(S24)} \\ &\leq 4 \left\| g_L(x) - \sqrt{\frac{1+f_K(x)}{2}} \right\|, & \text{(S25)} \\ &\leq \frac{\epsilon}{2}, & \text{(S26)} \end{aligned}$$

where $\|g_L(x)\| \leq 1$ and $\left\| \sqrt{\frac{1+f_K(x)}{2}} \right\| \leq 1$. Finally, combined with inequality (S19), inequality (S18) holds. ■

A.3 Proof of Lemma 3

Lemma 3 *There exists $\boldsymbol{\theta} = (\theta_0, \theta_1, \ldots, \theta_L) \in \mathbb{R}^{L+1}$ and $\boldsymbol{\phi} = (\phi_0, \phi_1, \ldots, \phi_L) \in \mathbb{R}^{L+1}$ such that*

$$U^{WZW}_{\boldsymbol{\theta},\boldsymbol{\phi},L}(x) = \begin{bmatrix} P & -Q \\ Q^* & P^* \end{bmatrix} \tag{S27}$$

if and only if Laurent polynomials $P, Q \in \mathbb{C}[e^{ix/2}, e^{-ix/2}]$ satisfy

1. $\deg(P) = \deg(Q) \leq L$,
2. *P and Q have parity $L \pmod 2$,*
3. $\forall x \in \mathbb{R}$, $|P|^2 + |Q|^2 = 1$.

Proof The entire proof is similar as the proof of Lemma 1, and the only difference is that the coefficients of Laurent polynomials could be complex rather than real. First we prove the forward direction by induction on L. For the base case, if $L = 0$, then $W(\theta_0, \phi_0) = R_Y(\theta_0) R_Z(\phi_0)$ gives $P = e^{-i\frac{\phi_0}{2}} \cos(\theta_0/2)$ and $Q = e^{i\frac{\phi_0}{2}} \sin(\theta_0/2)$, which clearly satisfies the three conditions.

For the induction step, suppose Eq. (S27) satisfies the three conditions. Then

$$\begin{bmatrix} P & -Q \\ Q^* & P^* \end{bmatrix} R_Z(x) R_Y(\theta_k) R_Z(\phi_k) \tag{S28}$$

$$= \begin{bmatrix} P & -Q \\ Q^* & P^* \end{bmatrix} \begin{bmatrix} \cos\frac{\theta_k}{2} e^{-i\frac{\phi_k}{2}} e^{-i\frac{x}{2}} & -\sin\frac{\theta_k}{2} e^{i\frac{\phi_k}{2}} e^{-i\frac{x}{2}} \\ \sin\frac{\theta_k}{2} e^{-i\frac{\phi_k}{2}} e^{i\frac{x}{2}} & \cos\frac{\theta_k}{2} e^{i\frac{\phi_k}{2}} e^{i\frac{x}{2}} \end{bmatrix} \tag{S29}$$

$$= \begin{bmatrix} \cos\frac{\theta_k}{2} e^{-i\frac{\phi_k}{2}} e^{-i\frac{x}{2}} P - \sin\frac{\theta_k}{2} e^{-i\frac{\phi_k}{2}} e^{i\frac{x}{2}} Q & -\sin\frac{\theta_k}{2} e^{i\frac{\phi_k}{2}} e^{-i\frac{x}{2}} P - \cos\frac{\theta_k}{2} e^{i\frac{\phi_k}{2}} e^{i\frac{x}{2}} Q \\ \cos\frac{\theta_k}{2} e^{-i\frac{\phi_k}{2}} e^{-i\frac{x}{2}} Q^* + \sin\frac{\theta_k}{2} e^{-i\frac{\phi_k}{2}} e^{i\frac{x}{2}} P^* & \cos\frac{\theta_k}{2} e^{i\frac{\phi_k}{2}} e^{i\frac{x}{2}} P^* - \sin\frac{\theta_k}{2} e^{i\frac{\phi_k}{2}} e^{-i\frac{x}{2}} Q^* \end{bmatrix} \tag{S30}$$

$$= \begin{bmatrix} \bar{P} & -\bar{Q} \\ \bar{Q}^* & \bar{P}^* \end{bmatrix} \tag{S31}$$

where

$$\bar{P} = \cos\frac{\theta_k}{2} e^{-i\frac{\phi_k}{2}} e^{-i\frac{x}{2}} P - \sin\frac{\theta_k}{2} e^{-i\frac{\phi_k}{2}} e^{i\frac{x}{2}} Q, \tag{S32}$$

$$\bar{Q} = \sin\frac{\theta_k}{2} e^{i\frac{\phi_k}{2}} e^{-i\frac{x}{2}} P + \cos\frac{\theta_k}{2} e^{i\frac{\phi_k}{2}} e^{i\frac{x}{2}} Q \tag{S33}$$

clearly satisfy the first condition $\deg(\bar{P}) = \deg(\bar{Q}) \leq L + 1$. They also satisfy the second condition since multiplying by $e^{-ix/2}$ or $e^{ix/2}$ alters the parity. The third condition is satisfied because of unitarity.

Next we show the backward direction by induction on L that the three conditions suffice to construct the QNN in Eq. (S27). First we consider the base case of $L = 0$, we have $\deg(P) = \deg(Q) = 0$, the above condition implies that $P = e^{-i\phi_0/2}\cos(\theta_0/2)$ and $Q = e^{i\phi_0/2}\sin(\theta_0/2)$ for some $\theta_0, \phi_0 \in \mathbb{R}$. Thus the matrix

$$\begin{bmatrix} P & -Q, \\ Q^* & P^* \end{bmatrix} \tag{S34}$$

can be written as a QNN $U^{WZW}_{\boldsymbol{\theta},\boldsymbol{\phi},L}(x) = R_Y(\theta_0) R_Z(\phi_0)$.

For the induction step, suppose Laurent polynomials P and Q satisfy the three conditions for some $L > 0$. We first observe that condition 3 implies

$$|P|^2 + |Q|^2 = PP^* + QQ^* = 1, \tag{S35}$$

where $PP^* + QQ^*$ is a polynomial in $e^{ix/2}$ with parity $2n \pmod 2 = 0$. Since Eq. (S35) holds for all $x \in \mathbb{R}$, the leading coefficients must satisfy $p_d p^*_{-d} + q_d q^*_{-d} = 0$ and $p^*_d p_{-d} + q^*_d q_{-d} = 0$, where $d \coloneqq \deg(P) = \deg(Q)$. By the first condition, we have $d \leq L$. We choose $\theta_k, \phi_k \in \mathbb{R}$ so that

$$\cos\frac{\theta_k}{2} e^{i\frac{\phi_k}{2}} p_d + \sin\frac{\theta_k}{2} e^{-i\frac{\phi_k}{2}} q_d = 0, \tag{S36}$$

$$-\sin\frac{\theta_k}{2} e^{i\frac{\phi_k}{2}} p_{-d} + \cos\frac{\theta_k}{2} e^{-i\frac{\phi_k}{2}} q_{-d} = 0. \tag{S37}$$

Now we briefly argue that there always exists θ_k and ϕ_k satisfy equations above. If all p_d, p_{-d}, q_d, q_{-d} are not zero, simply let $\tan\left(\frac{\theta_k}{2}\right) e^{-i\phi_k} = -\frac{p_d}{q_d}$. Then consider the case of zero coefficients. Since $\deg(P) = \deg(Q) = d$, at most two of p_d, p_{-d}, q_d, q_{-d} could be 0. The fact $p_d p^*_{-d} + q_d q^*_{-d} = 0$ implies that one of one of p_d, p_{-d} is 0 if and only if one of q_d, q_{-d} is 0. If $p_d = q_d = 0$ (or $p_{-d} = q_{-d} = 0$), pick θ_k and ϕ_k so that $\tan\left(\frac{\theta_k}{2}\right) e^{i\phi_k} = \frac{q_{-d}}{p_{-d}}$. If $p_d = q_{-d} = 0$ or ($p_{-d} = q_d = 0$), pick θ_k so that $\sin\left(\frac{\theta_k}{2}\right) = 0$ (or $\cos\left(\frac{\theta_k}{2}\right) = 0$).

Next, for the θ_k that we pick, consider

$$\begin{bmatrix} P & -Q \\ Q^* & P^* \end{bmatrix} W^\dagger(\theta_k, \phi_k) R_Z^\dagger(x) \tag{S38}$$

$$= \begin{bmatrix} e^{i\frac{\phi_k}{2}} \cos\frac{\theta_k}{2} e^{i\frac{x}{2}} P + e^{-i\frac{\phi_k}{2}} \sin\frac{\theta_k}{2} e^{i\frac{x}{2}} Q & e^{i\frac{\phi_k}{2}} \sin\frac{\theta_k}{2} e^{-i\frac{x}{2}} P - e^{-i\frac{\phi_k}{2}} \cos\frac{\theta_k}{2} e^{-i\frac{x}{2}} Q \\ e^{i\frac{\phi_k}{2}} \cos\frac{\theta_k}{2} e^{i\frac{x}{2}} Q^* - e^{-i\frac{\phi_k}{2}} \sin\frac{\theta_k}{2} e^{i\frac{x}{2}} P^* & e^{-i\frac{\phi_k}{2}} \cos\frac{\theta_k}{2} e^{-i\frac{x}{2}} P^* + e^{i\frac{\phi_k}{2}} \sin\frac{\theta_k}{2} e^{-i\frac{x}{2}} Q^* \end{bmatrix} \tag{S39}$$

$$= \begin{bmatrix} \hat{P} & -\hat{Q} \\ \hat{Q}^* & \hat{P}^* \end{bmatrix} \tag{S40}$$

where

$$\hat{P} = e^{i\frac{\phi_k}{2}} \cos\frac{\theta_k}{2} e^{i\frac{x}{2}} P + e^{-i\frac{\phi_k}{2}} \sin\frac{\theta_k}{2} e^{i\frac{x}{2}} Q, \tag{S41}$$

$$\hat{Q} = e^{-i\frac{\phi_k}{2}} \cos\frac{\theta_k}{2} e^{-i\frac{x}{2}} Q - e^{i\frac{\phi_k}{2}} \sin\frac{\theta_k}{2} e^{-i\frac{x}{2}} P. \tag{S42}$$

Since $P, Q \in \mathbb{C}[e^{ix/2}, e^{-ix/2}]$ are Laurent polynomials with degree d, $\hat{P} \in \mathbb{R}[e^{ix/2}, e^{-ix/2}]$ might appear to be a Laurent polynomial with degree $d+1$. In fact it has degree $\deg(\hat{P}) \leq d-1$, because the coefficient of $(e^{i\frac{x}{2}})^{d+1}$ term in $\hat{P}$ is $\cos\frac{\theta_k}{2} e^{i\frac{\phi_k}{2}} p_d + \sin\frac{\theta_k}{2} e^{-i\frac{\phi_k}{2}} q_d = 0$ by the selected θ_k and ϕ_k, and the coefficients of $(e^{\frac{ix}{2}})^d$ term is 0 by condition 2. Similarly, $\hat{Q}$ has leading coefficient $-\sin\frac{\theta_k}{2} e^{i\frac{\phi_k}{2}} p_{-d} + \cos\frac{\theta_k}{2} e^{-i\frac{\phi_k}{2}} q_{-d} = 0$ and has degree $\deg(\hat{Q}) \leq d-1$. Since $d \leq L$, we have $\deg(\hat{P}) = \deg(\hat{Q}) \leq L-1$, hence condition 1 is satisfied. From the parity of P and Q, it is easy to see that $\hat{P}$ and $\hat{Q}$ have parity $L-1 \pmod 2$, thus condition 2 is satisfied. Condition 3 follows from unitarity. Thus by the induction hypothesis, Eq. (S40) can be written as a QNN in the form of $U^{WZW}_{\boldsymbol{\theta},\boldsymbol{\phi},L-1}(x)$, and therefore the matrix

$$\begin{bmatrix} P & -Q \\ Q^* & P^* \end{bmatrix} \tag{S43}$$

can be written as a QNN in the form of $U^{WZW}_{\boldsymbol{\theta},\boldsymbol{\phi},L}(x)$. ■

A.4 Proof of Theorem 4

Theorem 4 (Univariate approximation properties of single-qubit QNNs.) *For any univariate square-integrable function $f : [-\pi, \pi] \to [-1, 1]$ and for all $\epsilon > 0$, there exists a QNN $U^{WZW}_{\boldsymbol{\theta},\boldsymbol{\phi},L}(x)$ such that $|\psi(x)\rangle = U^{WZW}_{\boldsymbol{\theta},\boldsymbol{\phi},L}(x)\,|0\rangle$ satisfies*

$$\|\langle\psi(x)|Z|\psi(x)\rangle - f(x)\| \leq \epsilon. \tag{S44}$$

Proof Similar as in the proof of Proposition 2, we use the fact that square-integrable functions f can be approximated by a truncated Fourier series. Then, there exists a $K \in \mathbb{N}^+$ such that

$$\|f_K(x) - f(x)\| \leq \frac{\epsilon}{2}, \tag{S45}$$

where $f_K(x)$ is the K-term truncated Fourier series of $f(x)$. Consider the function $\sqrt{\frac{1+f_K(x)}{2}}$, using the property of square-integrable functions again, there exists an $L \in \mathbb{N}^+$ such that

$$\left\| g_L(x) - \sqrt{\frac{1+f_K(x)}{2}} \right\| \leq \frac{\epsilon}{8}, \tag{S46}$$

where

$$g_L(x) = \sum_{n=-L/2}^{L/2} c_n e^{inx} \tag{S47}$$

is the partial Fourier series of function $\sqrt{\frac{1+f_K(x)}{2}}$ and $L \pmod 2 = 0$. Next we need to prove

$$\langle 0|U^{WZW}_{\boldsymbol{\theta},\boldsymbol{\phi},L}(x)|0\rangle = g_L(x). \tag{S48}$$

Specifically, $g_L(x)$ can be written as follows

$$g_L(x) = \sum_{n=-L/2}^{L/2} c_n (e^{ix/2})^{2n}. \tag{S49}$$

Obviously, $g_L \in \mathbb{C}[e^{ix/2}, e^{-ix/2}]$ and conditions of Lemma 3 are satisfied, thus Eq. (S48) holds. Further, we have

$$\| \langle \psi(x)|Z|\psi(x)\rangle - f_K(x)\| \leq \frac{\epsilon}{2}. \tag{S50}$$

Finally, combined with inequality (S45), the inequality (S44) holds. ■

B Fourier frequency and encoding block

In this section, we show that if the single-qubit native QNN is written in the form of a K-truncated multivariate Fourier series, it has a rich Fourier frequency set Ω, but it cannot meet the requirements of the corresponding Fourier coefficients set C_Ω due to the curse of dimensionality. Specifically, let $\boldsymbol{x} := (x^{(1)}, x^{(2)}, \ldots, x^{(d)}) \in \mathbb{R}^d$ and the single-qubit native QNN is defined as follows:

$$U_{\boldsymbol{\theta},L}(\boldsymbol{x}) = U_3(\theta_0, \phi_0, \lambda_0) \prod_{j=1}^{L} R_Z(x_j) U_3(\theta_j, \phi_j, \lambda_j), \tag{S51}$$

where x_j is a one-dimensional data of $\boldsymbol{x}$, i.e., $x_j \in \{x^{(m)} \mid m = 1, \cdots, d\}$. The quantum circuit is shown in Fig. S1.

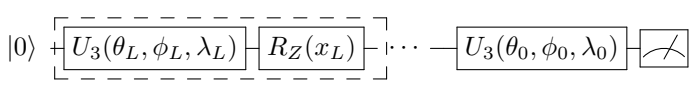

Figure S1: Circuit of $U_{\boldsymbol{\theta},L}(\boldsymbol{x})$, where the trainable block is composed of $U_3(\cdot)$, and the encoding block is $R_Z(\cdot)$. Note that there is no restriction on the encoding order of $x^{(m)}$.

Without loss of generality, assume that each one-dimensional data $x^{(m)}$ is uploaded the same number of times, denoted by K, then we have $Kd = L$. Further, we write $V_j := U_3(\theta_j, \phi_j, \lambda_j)$ for short, that is

$$U_{\boldsymbol{\theta},L}(\boldsymbol{x}) = V_0 \prod_{j=1}^{L} \begin{bmatrix} e^{-ix_j\lambda_0} & 0 \\ 0 & e^{-ix_j\lambda_1} \end{bmatrix} V_j, \tag{S52}$$

where $\lambda_0 = \frac{1}{2}$ and $\lambda_1 = -\frac{1}{2}$. More generally, we have

$$U_{\boldsymbol{\theta},L}(\boldsymbol{x}) = \sum_{j_1,\cdots,j_L=0}^{1} e^{-i(\lambda_{j_1}x_1+\cdots+\lambda_{j_L}x_L)} V_0 |j_1\rangle\langle j_1| V_1 \cdots |j_L\rangle\langle j_L| V_L. \tag{S53}$$

Next, we reformulate the above equation using $x^{(m)}$ instead of x_j. We denote $I_m \subset \{1, \cdots, L\}$ as the index set of encoding block $R_Z(x^{(m)})$ and $I'_m = \{\lambda_{j_k} \mid k \in I_m\}$, then

$$U_{\boldsymbol{\theta},L}(\boldsymbol{x}) = \sum_{\boldsymbol{j}\in\{0,1\}^L} e^{-i(\Lambda^{(1)}_{\boldsymbol{j}}x^{(1)}+\cdots+\Lambda^{(d)}_{\boldsymbol{j}}x^{(d)})} V_0 |j_1\rangle\langle j_1| V_1 \cdots |j_L\rangle\langle j_L| V_L, \tag{S54}$$

where $\boldsymbol{j}$ is bit-strings composed of j_l, $l = 1, \cdots, L$ and $\Lambda^{(m)}_{\boldsymbol{j}} = \sum \lambda$, $\lambda \in I'_m$. Further, for the initial state $|0\rangle$ and some observable M, we have

$$f_{\boldsymbol{\theta},L}(\boldsymbol{x}) = \langle 0| U^\dagger_{\boldsymbol{\theta},L}(\boldsymbol{x}) M U_{\boldsymbol{\theta},L}(\boldsymbol{x}) |0\rangle = \sum_{\boldsymbol{\omega}\in\Omega} c_{\boldsymbol{\omega}} e^{i\boldsymbol{\omega}\cdot\boldsymbol{x}}, \tag{S55}$$

where $\Omega = \{h_{\boldsymbol{j},\boldsymbol{k}} := (\Lambda_{\boldsymbol{k}}^{(1)} - \Lambda_{\boldsymbol{j}}^{(1)}, \cdots, \Lambda_{\boldsymbol{k}}^{(d)} - \Lambda_{\boldsymbol{j}}^{(d)}) \mid \boldsymbol{j}, \boldsymbol{k} \in \{0,1\}^L\}$. We consider the m-th dimension,

$$\Lambda_{\boldsymbol{k}}^{(m)} - \Lambda_{\boldsymbol{j}}^{(m)} = \{(\lambda_{k_1} + \cdots + \lambda_{k_K}) - (\lambda_{j_1} + \cdots + \lambda_{j_K}) \mid \lambda_{k_1} \cdots \lambda_{k_K}, \lambda_{j_1} \cdots \lambda_{j_K} \in I'_m\}. \tag{S56}$$

Since $\lambda = \pm\frac{1}{2}$, for all $\lambda \in I'_m$, we can derive

$$\{\Lambda_{\boldsymbol{k}}^{(m)} - \Lambda_{\boldsymbol{j}}^{(m)} \mid \boldsymbol{j}, \boldsymbol{k} \in \{0,1\}^L\} = \{-K, \cdots, 0, \cdots, K\}. \tag{S57}$$

Then the Fourier frequency spectrum is $\Omega = \{-K, \cdots, 0, \cdots, K\}^d$. For the Fourier coefficient set $C_\Omega = \{c_{\boldsymbol{\omega}} \mid \boldsymbol{\omega} \in \Omega\}$, we have

$$c_{\boldsymbol{\omega}} = \sum_{\boldsymbol{j},\boldsymbol{k} \in \{0,1\}^L, \boldsymbol{\omega} = h_{\boldsymbol{j},\boldsymbol{k}}} C_{\boldsymbol{j},\boldsymbol{k}}, \tag{S58}$$

and

$$C_{\boldsymbol{j},\boldsymbol{k}} = \langle 0| V_L^\dagger |k_L\rangle\langle k_L| V_{L-1}^\dagger \cdots |k_1\rangle\langle k_1| V_1^\dagger M V_1 |j_1\rangle\langle j_1| \cdots V_{L-1} |j_L\rangle\langle j_L| V_L |0\rangle. \tag{S59}$$

If the number of truncation terms K is fixed, as the dimension d increases, the degrees of freedom of the set C_Ω increase with $O(d)$, so it cannot represent any exponential size Fourier coefficients set. Thus for all $\boldsymbol{\theta} \in \mathbb{R}^{3(L+1)}$, the Eq. (S55) cannot express an arbitrary k-truncated multivariate Fourier series.

C Extension to multi-qubit QNNs

We have already shown that single-qubit native QNNs are able to approximate any univariate function but possibly could not approximate arbitrary multivariate functions by Fourier series in Section 3 and Section 4. To address this limitation, research into the extension approach of single-qubit native QNNs is crucial. For classical NNs, a common approach toward overcoming such limitations is to increase the width or depth of the networks. We conjecture that QNNs have similar characteristics. We hereby provide a multi-qubit extension strategy as shown in Fig. S2, called *Parallel-Entanglement*, introducing quantum entanglement by multi-qubit gates such as CNOT gates. Similar to classical NNs in which different neurons are connected by trainable parameters to form deep NNs, QNNs can establish the connection between different qubits through quantum entanglement.

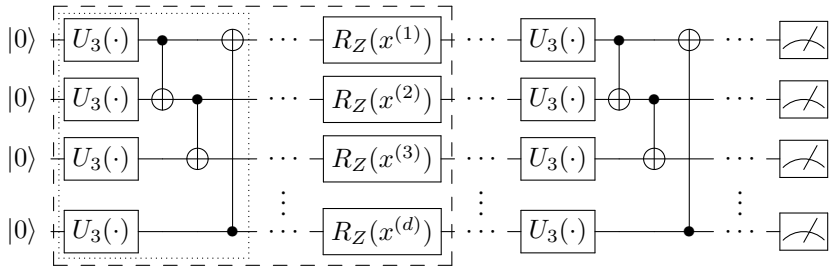

Figure S2: The Parallel-Entanglement model of d qubits and L layers. Each layer consists of a trainable block and an encoding block in the dashed box. Each trainable block is composed of repeated sub-blocks of U_3 rotation gates and CNOT gates, as shown in the dotted box. The number of sub-blocks in each trainable block is denoted by D_{tr}. The encoding block is a d-tensor of $R_Z(x^{(m)})$ gates for a d-dimensional data $\boldsymbol{x} := (x^{(1)}, \ldots, x^{(d)})$.

We numerically show that the multi-qubit extension as shown in Fig. S2 could improve the expressivity of single-qubit QNNs. Consider the same bivariate function $f(x, y) = (x^2+y-1.5\pi)^2+(x+y^2-\pi)^2$ used in Section 5.2, we use a two-qubit QNN of $L = 10$ and $D_{tr} = 3$ to approximate the target function $f(x, y)$ with the same training setting. The experimental results are shown in Fig. S3. Compared with the approximation results of single-qubit QNNs in Fig. 6, we can see that the two-qubit QNN has stronger expressive power than single-qubit models. Moreover, we could build the *universal trainable block* (UTB) using a universal two-qubit quantum gate [37, 38] consisting of

U_3 and CNOT gates. Specifically, a two-qubit universal trainable block can express any two-qubit unitary matrix. Using a two-qubit QNN with UTBs yields a better approximation result which is shown in Fig. S4. From the numerical results, we could see that the multi-qubit extension could potentially overcome the limitations of single-qubit QNNs on approximating multivariate functions as illustrated in Section 4.

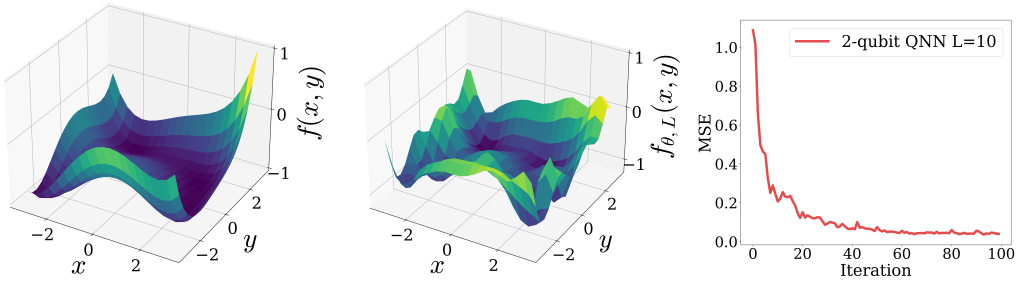

(a) Target function. (b) Approximation result. (c) Training loss.

Figure S3: Panel (a) is the plot of target function $f(x, y)$. Panel (b) shows the approximation result of a two-qubit QNN of $L = 10$ and $D_{tr} = 3$. Panel (c) is the plot of training loss during the optimization.

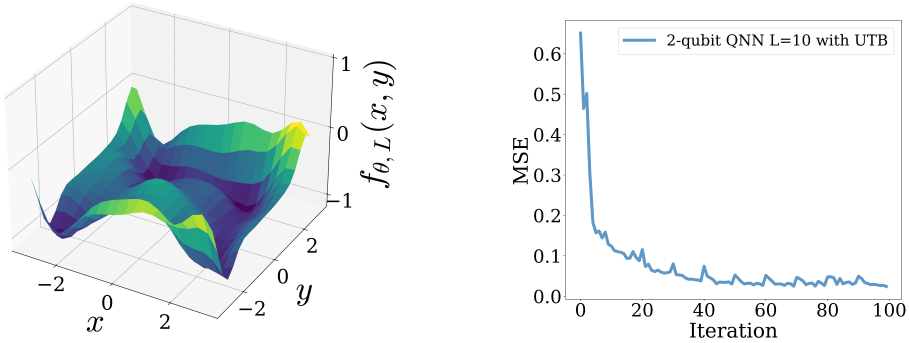

(a) Approximation result. (b) Training loss.

Figure S4: Panel (a) shows the approximation result of a two-qubit QNN of $L = 10$ with UTB. Panel (b) is the plot of training loss during the optimization.

We further illustrate the ability of Parallel-Entanglement models to address practical problems through experiments on the classification task. The public benchmark data sets are used to demonstrate the capabilities of Parallel-Entanglement models to tackle classification tasks.

Table 1: The performance of the Parallel-Entanglement model.

Dataset	**# of qubits**	L	D_{tr}	**# of parameters**	**Average accuracy**
Iris	4	1	1	16	0.990 ± 0.01
HTRU2	8	1	1	32	0.910 ± 0.09
		3	1	64	0.970 ± 0.03
		3	2	128	0.980 ± 0.02
Breast Cancer	4	1	1	16	0.780 ± 0.06
		3	1	32	0.840 ± 0.02
		3	2	64	0.845 ± 0.04

The performance of the Parallel-Entanglement model on classifying Iris [39], Breast Cancer [40], and HTRU2 [41] data sets are summarized in Table 1. Specifically, 100 pieces of data are sampled from

the dataset, with 80% of them serving as the training set and 20% serving as the test set. We use the Adam optimizer with a learning rate of 0.1 and a batch size of 40 to train the multi-qubit QNNs. In order to reduce the effect of randomness, the results of classification accuracy are averaged over 10 independent training instances.

The Iris data set contains 3 different classes, each class only has four attributes. Obviously, the 4-qubit model easily obtains an average accuracy of over 99% with only 1 layer on Iris data. The HTRU2 data set only has two categories, and each example has 8 attributes. As a result, an 8-qubit QNN is required to complete this task. The average accuracy for binary classification with 1 layer achieves above 91%. We can see that adding the number of layers to 3 and the depth of each layer to 2 increases the average accuracy to 98%. Since the Breast Cancer data contains 30 features for binary classification, the principal component analysis (PCA) is used to reduce feature dimension. Here the numerical results of a 4-qubit model are given to illustrate the power of the QNN. Compared to the model using complete information, the QNN model does not perform perfectly. But increasing the number of layers and the depth may improve the test accuracy. Based on the finding of the preceding experiments, it is clear that the Parallel-Entanglement model is capable of handling practical classification problems.